LETTERS
https://doi.org/10.1038/s41563-018-0061-1
nature materials

An unusual continuous paramagnetic-limited superconducting phase transition in 2D $NbSe_2$

Egon Sohn[1,2], Xiaoxiang Xi[1,3], Wen-Yu He[4], Shengwei Jiang[1,2], Zefang Wang[1,2], Kaifei Kang[1,2], Ju-Hyun Park[5], Helmuth Berger[6], László Forró[6], Kam Tuen Law[4], Jie Shan[1,2,7]* and Kin Fai Mak[1,2,7]*

Time reversal and spatial inversion are two key symmetries for conventional Bardeen–Cooper–Schrieffer (BCS) superconductivity[1]. Breaking inversion symmetry can lead to mixed-parity Cooper pairing and unconventional superconducting properties[1–5]. Two-dimensional (2D) $NbSe_2$ has emerged as a new non-centrosymmetric superconductor with the unique out-of-plane or Ising spin–orbit coupling (SOC)[6–9]. Here we report the observation of an unusual continuous paramagnetic-limited superconductor–normal metal transition in 2D $NbSe_2$. Using tunelling spectroscopy under high in-plane magnetic fields, we observe a continuous closing of the superconducting gap at the upper critical field at low temperatures, in stark contrast to the abrupt first-order transition observed in BCS thin-film superconductors[10–12]. The paramagnetic-limited continuous transition arises from a large spin susceptibility of the superconducting phase due to the Ising SOC. The result is further supported by self-consistent mean-field calculations based on the ab initio band structure of 2D $NbSe_2$. Our findings establish 2D $NbSe_2$ as a promising platform to explore novel spin-dependent superconducting phenomena and device concepts[1], such as equal-spin Andreev reflection[13] and topological superconductivity[14–16].

In conventional BCS superconductors, Cooper pairs are even-parity singlets[17], which yield a nearly zero spin susceptibility at low temperatures. The paramagnetic-limited superconductor-normal metal transition is thus an abrupt first-order transition at the upper critical field[10] (Fig. 1a). This has been verified experimentally, for instance, in very thin superconducting aluminium[10,11] and beryllium[12] films under an in-plane magnetic field, for which orbital depairing is suppressed. In non-centrosymmetric superconductors, which lack a center of inversion in the crystal structure, the presence of antisymmetric SOC can give rise to a wealth of novel properties, including the superconducting magnetoelectric effect[1], spin Hall effect[1] and helical phases[1,18]. In particular, the spin susceptibility of the superconducting phase can become significant compared to the normal-state value[19–21] and lead to a continuous paramagnetic-limited transition in the zero-temperature limit[22] (Fig. 1a). Such a transition, however, has not yet been observed in any systems. The recently emerged non-centrosymmetric superconductors 2D $NbSe_2$ (refs [6–9]) and gated MoS_2 (refs [23,24]) possess unique Ising SOC, which pins the electron spins to the out-of-plane direction. They also have a sample thickness much smaller than the bulk penetration depth, and therefore a significantly suppressed orbital response to an in-plane magnetic field[7,9,23,25]. In contrast to the well-known non-centrosymmetric superconductors with a Rashba SOC[1–5], in which the orbital effect is often important, atomically thin superconductors with an Ising SOC provide an ideal platform for the investigation of the paramagnetic-limited phase transition and other pure spin-dependent superconducting phenomena and device concepts.

Single-layer $NbSe_2$ consists of a layer of Nb atoms sandwiched between two layers of Se atoms in a trigonal prismatic structure[9,26]. It has out-of-plane mirror symmetry and broken inversion symmetry. Electrons are subject to strong out-of-plane SOC fields (opposite at opposing crystal momenta), and are effectively Ising spins[9,13,23,24]. The Ising spins are largely preserved in each monolayer of multilayer samples due to the weak interlayer interactions[9] (Fig. 1b). Recent experimental advances in high-quality atomically thin $NbSe_2$ samples have unveiled the coexistence of charge-density-wave order and superconductivity down to the monolayer limit[8,26], in-plane upper critical fields that far exceed the spin paramagnetic limit of the BCS theory[9] and a Bose metal phase[7]. The earlier studies[9,23,24] based on resistance measurements, however, do not have direct access to the spectroscopic information and the superconducting order parameter[13,15,18]. Here we report the tunelling measurement and the observation of an unusual continuous paramagnetic-limited phase transition in 2D $NbSe_2$ in the paramagnetic-limited regime. Our result provides strong evidence for a significant spin susceptibility of the superconducting phase in the zero-temperature limit originated from the Ising SOC.

Figure 1c shows the optical image and energy diagram of a typical normal metal–insulator–superconductor (NIS) junction employed in this experiment. It consists of a thin layer of platinum or gold electrode, a thin layer of tunnel barrier and a superconducting $NbSe_2$ layer. Two different tunnel barrier materials, aluminium oxide (AlO_x) and few-layer MoS_2, were tested. Both types yielded similar results. Bilayer and trilayer instead of monolayer $NbSe_2$ were studied because of their significantly higher chemical stabilities and sheet-critical current densities. The weak interlayer interactions mean the results for atomically thin samples are similar. Below we present the trilayer result and include the bilayer result in Supplementary Sections 4 and 5. Both the four-point resistance R and the differential tunelling conductance spectrum $G(V)$ ($=dI/dV$, where I is the tunelling current and V is the bias voltage) were measured on the same devices. These quantities, normalized by the

[1]Department of Physics, The Pennsylvania State University, University Park, PA, USA. [2]Department of Physics and School of Applied and Engineering Physics, Cornell University, Ithaca, NY, USA. [3]National Laboratory of Solid State Microstructures, School of Physics, and Collaborative Innovation Center of Advanced Microstructures, Nanjing University, Nanjing, China. [4]Department of Physics, Hong Kong University of Science and Technology, Clear Water Bay, Hong Kong, China. [5]National High Magnetic Field Laboratory, Florida State University, Tallahassee, FL, USA. [6]Institute of Condensed Matter Physics, Ecole Polytechnique Fédérale de Lausanne, Lausanne, Switzerland. [7]Kavli Institute at Cornell for Nanoscale Science, Ithaca, NY, USA. *e-mail: jie.shan@cornell.edu; kinfai.mak@cornell.edu

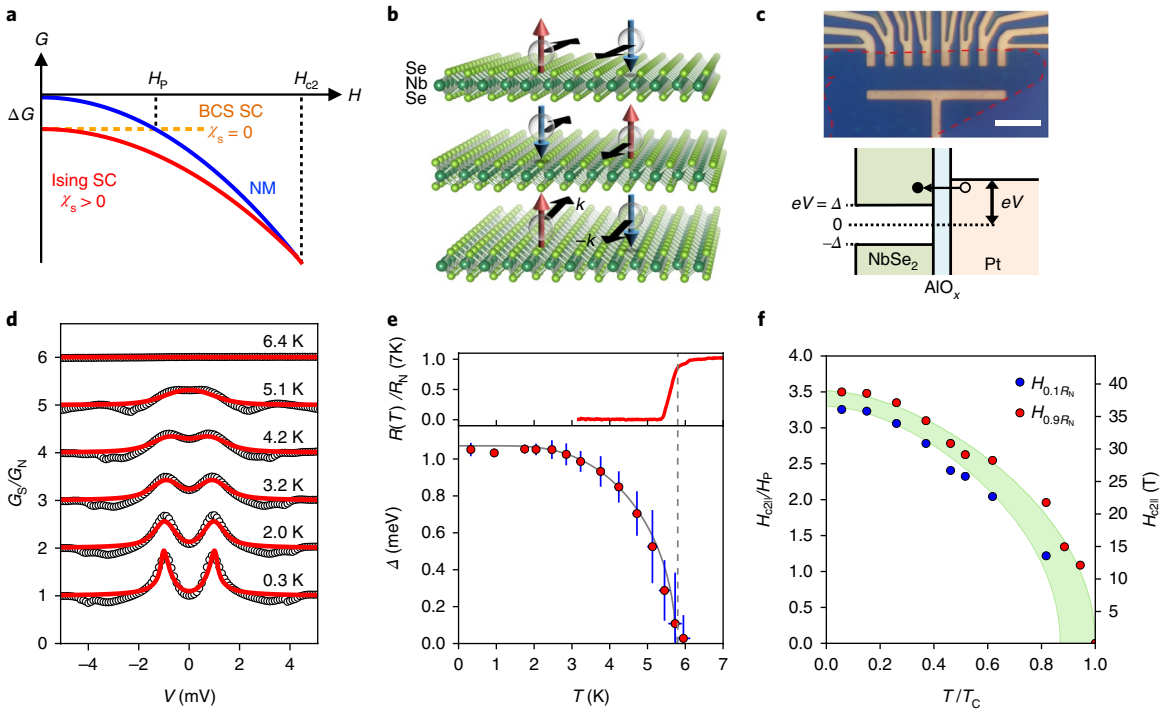

Fig. 1 | 2D $NbSe_2$ superconductor tunnel junction. a, Magnetic-field dependence of the free energy of a normal metal (NM) (blue line), BCS superconductor (SC) (orange dashed line) and an Ising SC (red line). ΔG is the condensation energy. The paramagnetic-limited transition is first order at H_P if the spin susceptibility $\chi_s = 0$ (BCS SC), and second order at a higher upper critical field H_{c2} if the spin susceptibility is significant $\chi_s > 0$ (Ising SC). **b**, Schematic of Ising spins in a superconducting trilayer of $NbSe_2$. In each monolayer, electrons of the K and K′ pocket possess opposite momentum k and $-k$ (in-plane arrows) and opposite spin (out-of-plane arrows). Electrons of the same momentum in adjacent weakly coupled layers have opposite spins because the two layers are inverted. **c**, Optical image of a typical $NbSe_2$ tunnel junction (top). It consists of Pt electrodes (yellow), a thin layer of AlO_x, a $NbSe_2$ superconductor (outlined by red dashed lines) and a hBN capping layer (blue). Scale bar, 10 μm. The energy diagram of the junction (bottom) shows that the tunnelling current as a function of bias voltage V measures the superconducting gap 2Δ, and e is the elementary charge. **d**, Differential tunnelling conductance spectra (open circles) and comparison to the BTK model (red lines) of trilayer $NbSe_2$ at varying temperatures under zero magnetic field. **e**, Temperature dependence of the normalized four-point resistance (solid red line, upper panel) and the temperature dependence of the superconducting gap Δ from tunnelling measurements (red circles, lower panel). The vertical and horizontal error bars of Δ correspond to the BTK fitting error and sample-temperature fluctuations, respectively. The dashed line indicates the critical temperature T_C. The solid grey line is the prediction of the BCS theory with a zero-temperature gap $2\Delta_0 \approx 4.3 k_B T_C$. **f**, Temperature dependence of the critical field $H_{c2}^{\parallel}$ (red circles) and of the superconducting transition width (shaded region between 90% (red) and 10% (blue) of the normal-state resistance). The critical field and the sample temperature are normalized by the spin paramagnetic limit of the BCS theory $H_P = 10.8$ T and the critical temperature $T_C = 5.8$ K, respectively.

normal-state values (R_N and G_N), are shown in Figs. 1 and 2. Raw differential conductance spectra are included in Supplementary Section 4. Details on the device fabrication and electrical measurements are provided in Methods and Supplementary Sections 1–3.

The basic characterization of 2D $NbSe_2$ superconductors by four-point resistance measurements is shown in Fig. 1e,f. The critical temperature determined from the onset of the transition (90% of the normal resistance) is $T_C \approx 5.8$ K (Fig. 1e, top panel). The in-plane critical field $H_{c2}^{\parallel}$ determined from the onset of the transition increases with decreasing temperature and saturates at ~ 38 T (Fig. 1f). This value is about 3.5 times the Pauli paramagnetic limit H_P ($\approx 1.84\ T_C$) of the BCS theory[17], which supports the preserved Ising spins in trilayer $NbSe_2$ as a result of weak interlayer interactions[9]. Meanwhile, the transition width (shaded region of the fields between 90% and 10% of the normal-state resistance) increases with temperature due to the enhanced thermal fluctuations[10,17]. It approaches about 2 T at low temperatures, probably limited by sample inhomogeneities. These results agree well with reported studies[6,7,9,26].

We now investigate the superconducting gap as a function of temperature and in-plane field by tunnelling spectroscopy. The differential tunnelling conductance spectra under zero magnetic field are shown in Fig. 1d (open circles) for several representative temperatures. At low temperatures, they consist of two symmetric peaks that stem from the tunnelling of normal electrons into the electron and hole branches of the quasiparticles in the superconductor[17] (Fig. 1c). The separation between the peaks corresponds to the superconducting gap $2\Delta \approx 2$ meV. Finite in-gap conductance is also observed and is caused by Andreev reflection at junctions with a finite transparency[17,27]. As the temperature increases, the quasiparticle peaks broaden and their separation decreases, which indicates the closing of the superconducting gap. For a more quantitative analysis of the tunnelling spectra, we compare them to the Blonder–Tinkham–Klapwijk (BTK) model that includes both the single quasiparticle tunnelling and the Andreev process in an NIS junction of arbitrary barrier strength[17,27] (Fig. 1d, red lines). The dimensionless barrier strength, gap energy and quasiparticle lifetime were used as free fitting parameters. (Supplementary Sections 5.1 and 5.2 give the details). The agreement between experiment and theory is generally very good, except for the unaccounted small dips observed outside the superconducting gap. These features probably arise from the heating of local constrictions in the junction[27]. For typical junctions used in this experiment, the barrier strength (~0.5–1.5) is moderate. The temperature dependence of the gap is depicted in Fig. 1e (red circles) and can be described by the BCS theory[17] (Fig. 1e, grey line).

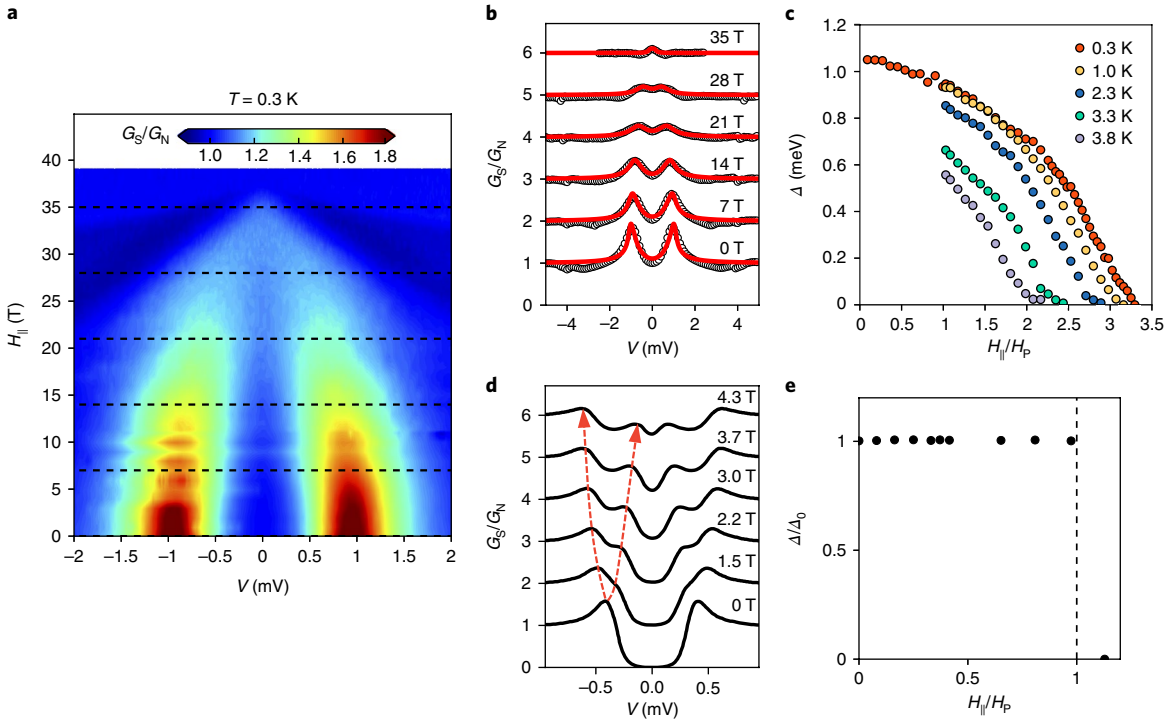

Fig. 2 | Tunnelling spectroscopy under in-plane magnetic fields. a, Contour plot of the differential conductance of trilayer $NbSe_2$ as a function of bias voltage (V) and in-plane field ($H_{||}$) at 0.3 K. A continuous closing of the superconducting gap is visible when the field is increased. **b**, Differential tunnelling conductance spectra (open circles) at selected fields (dashed lines in **a**) and comparison to the BTK model (red lines). The spectra are vertically displaced for clarity. **c**, The extracted superconducting gap from the tunnelling spectra as a function of field at differing temperatures. **d**,**e**, Tunnelling spectra at representative in-plane fields, vertically displaced for clarity (**d**), and field dependence of the superconducting gap (**e**) for aluminium thin films at low temperature are included for comparison. The dashed red lines in **d** illustrate the Zeeman splitting of the quasiparticle peak. Panel **d** adapted from ref. 11, American Physical Society.

Table 1 | Experimentally observed paramagnetic-limited superconductor–normal metal transitions

	Al (metal thin film)[10,11]	Be (metal thin film)[a] (ref. [12])	V-Ti (metal thin film)[10]	$CeCoIn_5$ (heavy fermion SC)[b,c] (refs [29,30])	κ-(*BEDT-TTF*)$_2$Cu(NCS)$_2$ (organic SC)[b] (ref. [31])	KFe_2As_2 (pnictide SC)[d,e] (ref. [32])	2D $NbSe_2$
H_{c2}/H_P	~1.0	~1.1	~1.1	~0.9	~1.0	~0.6	~3.5
Zeeman splitting	Y	-	Y	-	-	-	N
Phase-transition order ($T \approx 0$)	1st	1st	1st	1st	1st	1st	2nd

Experimental methods in addition to tunnelling measurements: [a]transport, [b]specific heat, [c]magnetization, [d]thermal expansion, [e]magnetostriction.

The extracted T_C (dashed vertical line) is consistent with the value from the resistance measurements. The extracted zero-temperature gap size $2\Delta_0 \approx 4.3 k_B T_C$ (where k_B is the Boltzmann constant) is higher than the usual $3.52 k_B T_C$ for a BCS superconductor[17], probably due to strong-coupling corrections[28].

The behaviour of the superconducting gap in an in-plane magnetic field is illustrated in Fig. 2. The contour plot in Fig. 2a is the differential conductance as a function of bias voltage V and in-plane field $H_{||}$ up to about 40 T at 0.3 K ($\approx 0.05 T_C$). Figure 2b shows the representative tunnelling spectra (open circles) together with a comparison to the BTK model (red lines). The BTK analysis here neglects both the orbital effect and the Zeeman effect (Methods gives a justification based on the estimated orbital-limited upper critical field). The extracted gap as a function of $H_{||}$ is summarized in Fig. 2c, and the other parameters in Supplementary Section 5.3. Figure 2c also includes results at several elevated temperatures. (Supplementary Section 5.5 gives raw spectra and an analysis.) For comparison, we include the classic example of superconducting aluminium thin films under an in-plane field[10,11] in Fig. 2d (tunnelling spectra) and Fig. 2e (superconducting gap extracted from published data[11] by our BTK analysis). Our results differ drastically from the behaviours of BCS thin-film superconductors: (1) the two quasiparticle peaks survived up to $H_{||} > 30$ T, which far exceeds the Pauli paramagnetic limit of the BCS superconductors[17]; (2) the two quasiparticle peaks exhibit negligible Zeeman splitting even under very high fields, unlike the significant Zeeman splitting observed in the BCS superconductors[10,11] and (3) as $H_{||}$ increases, the superconducting gap drops continuously to zero at the upper critical field in the zero-temperature limit, which indicates a continuous phase transition, in stark contrast to the abrupt first-order phase transition observed in BCS superconductors[10–12].

The observed continuous paramagnetic-limited superconductor–normal metal transition in 2D $NbSe_2$ is rather unique. Table 1 summarizes all currently available experiments on the order of the paramagnetic-limited transition. They range from metal thin films[10–12]

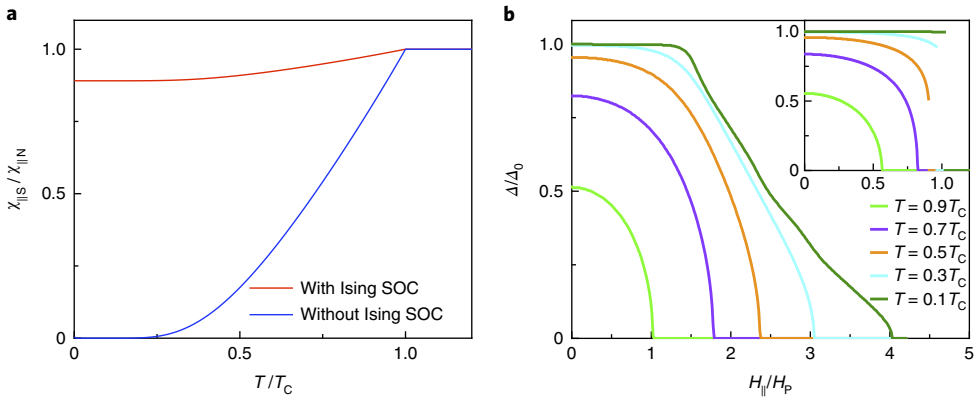

Fig. 3 | Calculations of the superconducting gap under in-plane magnetic fields. a, In-plane spin susceptibility of trilayer $NbSe_2$ normalized by the normal-state value ($\chi_{\|S}/\chi_{\|N}$) in the low-field limit as a function of temperature with (red line) and without (blue line) SOC. **b**, Superconducting gap normalized by the zero-temperature, zero-field value (Δ/Δ_0) as a function of the in-plane field at differing temperatures. The gap closes continuously with increasing field at all temperatures. Inset: the result without including SOC in the band structure of $NbSe_2$. The bandgap closes abruptly with increasing field at a low temperature ($0.1T_C$).

to quasi-2D heavy fermion[29,30], organic[31] and iron pnictide[32] systems such that orbital depairing is strongly suppressed under a magnetic field to reach the paramagnetic-limited regime. In the low-temperature limit, they all exhibit a first-order transition, in contrast to 2D $NbSe_2$. Note that non-centrosymmetric superconductors with Rashba SOC, in principle, can also exhibit a continuous paramagnetic-limited transition, but under an out-of-plane field (Supplementary Section 6.3). The orbital depairing under this configuration, however, makes it almost impossible to reach the paramagnetic-limited regime.

To understand our experimental observations, we consider the free energies of the normal and superconducting states in the zero-temperature limit when all real quasiparticle excitations are frozen. Including only the spin paramagnetic effect, the free energy can be expressed as $F_N = -\chi_{\|N} H_\|^2/2$ for the normal state, and $F_S = -N_0\Delta_0^2/2 - \chi_{\|S} H_\|^2/2$ for the superconducting state[1,17]. Here $\chi_{\|N}$ and $\chi_{\|S}$ denote the field-dependent spin susceptibility of the normal and superconducting states, respectively, and N_0 is the density of states at the Fermi surface. For a BCS superconductor, electron spins are Heisenberg like, that is, having no preferential direction. Under $H_\|$, the quasiparticle peaks are Zeeman split by $g\mu_B H_\|$ (refs [10,11]) (g and μ_B are the electron g-factor and the Bohr magneton, respectively). The spin susceptibility of the superconducting state is zero ($\chi_{\|S} = 0$) as the Cooper pairs are singlet[19,20]. The spin susceptibility of the normal state is the Pauli paramagnetic susceptibility $\chi_{\|N} = N_0(g\mu_B)^2/2$. The transition occurs when $F_S = F_N$ at the familiar upper critical field $H_{c2}^\| = H_P$. It is first order because the derivative of the two free energies is discontinuous at H_P (Fig. 1a)[10,12].

However, in 2D $NbSe_2$ with Ising spins pinned by the strong intralayer SOC field[9,13,15], $H_{SO} (\gg H_\|)$, the in-plane field induces an electron spin magnetic moment of $\sim g\mu_B \left(\frac{H_\|}{H_{SO}}\right)$ and a Zeeman splitting of $\sim g\mu_B H_\| \left(\frac{H_\|}{H_{SO}}\right) \ll g\mu_B H_\|$. This energy is ~ 0.1 meV even at $H_\| = 30$ T, which explains the negligible Zeeman splitting observed in the quasiparticle peaks. The Ising SOC also endows the in-plane spin susceptibility with a van Vleck character. The van Vleck spin susceptibility originates from virtual transitions that involve states over an energy scale much larger than that of the superconducting gap Δ_0 (ref. [22]) (the bandwidth, the spin–orbit splitting and Δ_0 of $NbSe_2$ are on the order of 1 eV, 100 meV and 1 meV, respectively[9]). As a result, the opening of a small superconducting gap at the Fermi surface has little effect on the spin susceptibility, that is, $\chi_{\|S} \approx \chi_{\|N}$ (refs [20,21]). The two free energies therefore touch smoothly to yield a continuous paramagnetic-limited transition at a much higher $H_{c2}^\|$ (Fig. 1a), as observed in our experiment.

Finally, we perform quantitative calculations of the superconducting gap as a function of the in-plane magnetic field in trilayer $NbSe_2$ to validate the above physical picture. The results were obtained by solving the self-consistent mean-field equation based on the ab initio band structure of trilayer $NbSe_2$ and on the assumption of an isotropic s-wave pairing potential[13,15]. The latter assumption is consistent with studies of the superconducting gap of bulk $NbSe_2$ by angle-resolved photoemission spectroscopy[33]. For comparison, we also included results with the Ising SOC turned off numerically. Figure 3a shows the temperature dependence of the ratio of the susceptibilities $\chi_{\|S}/\chi_{\|N}$ in the low-field limit. Whereas $\chi_{\|S}/\chi_{\|N}$ goes to zero at low temperatures in the absence of SOC, as expected for a BCS superconductor[19], $\chi_{\|S}/\chi_{\|N}$ remains close to unity even at low temperatures when SOC is included. Figure 3b depicts the field dependence of the gap. In the presence of SOC, the gap decreases to zero continuously with the field at all temperatures, in good agreement with our experiment (Fig. 2c). In contrast, the transition becomes first order at low temperatures in the absence of SOC (Fig. 3b, inset), in agreement with the behaviour of a BCS superconductor (Fig. 2e)[10–12].

In conclusion, we have observed an unusual continuous paramagnetic-limited superconductor–normal metal transition in 2D $NbSe_2$ at low temperatures by tunelling spectroscopy. Our results provide strong evidence for significant spin susceptibility of 2D $NbSe_2$ in the zero-temperature limit, which originates from the antisymmetric Ising SOC. The findings, together with the developed junction devices, pave the path to probe exotic superconducting phenomena, such as equal-spin Andreev reflection, proximity phenomena and topological superconductivity[13,15,16] in 2D $NbSe_2$.

Methods

Methods, including statements of data availability and any associated accession codes and references, are available at https://doi.org/10.1038/s41563-018-0061-1.

Received: 9 November 2017; Accepted: 16 March 2018;
Published online: 30 April 2018

References

1. Bauer, E. & Sigrist, M. *Non-centrosymmetric Superconductors: Introduction and Overview* (Springer, Berlin, Heidelberg, 2012).

2. Bauer, E. et al. Heavy fermion superconductivity and magnetic order in noncentrosymmetric $CePt_3Si$. *Phys. Rev. Lett.* **92**, 027003 (2004).
3. Yogi, M. et al. Evidence for novel pairing state in noncentrosymmetric superconductor $CePt_3Si$: ^{29}Si-NMR knight shift study. *J. Phys. Soc. Jpn.* **75**, 013709 (2006).
4. Yip, S. Noncentrosymmetric superconductors. *Annu. Rev. Condens. Matter Phys.* **5**, 15–33 (2014).
5. Smidman, M., Salamon, M. B., Yuan, H. Q. & Agterberg, D. F. Superconductivity and spin–orbit coupling in non-centrosymmetric materials: a review. *Rep. Progress. Phys.* **80**, 036501 (2017).
6. Cao, Y. et al. Quality heterostructures from two-dimensional crystals unstable in air by their assembly in inert atmosphere. *Nano Lett.* **15**, 4914–4921 (2015).
7. Tsen, A. W. et al. Nature of the quantum metal in a two-dimensional crystalline superconductor. *Nat. Phys.* **12**, 208–212 (2016).
8. Ugeda, M. M. et al. Characterization of collective ground states in single-layer $NbSe_2$. *Nat. Phys.* **12**, 92–97 (2016).
9. Xi, X. et al. Ising pairing in superconducting $NbSe_2$ atomic layers. *Nat. Phys.* **12**, 139–143 (2016).
10. Meservey, R. & Tedrow, P. M. Spin-polarized electron-tunneling. *Phys. Rep.* **238**, 173–243 (1994).
11. Meservey, R., Tedrow, P. M. & Bruno, R. C. Tunneling measurements on spin-paired superconductors with spin–orbit scattering. *Phys. Rev. B* **11**, 4224–4235 (1975).
12. Adams, P. W., Herron, P. & Meletis, E. I. First-order spin-paramagnetic transition and tricritical point in ultrathin Be films. *Phys. Rev. B* **58**, R2952–R2955 (1998).
13. Zhou, B. T., Yuan, N. F., Jiang, H.-L. & Law, K. T. Ising superconductivity and Majorana fermions in transition-metal dichalcogenides. *Phys. Rev. B* **93**, 180501 (2016).
14. Yuan, N. F., Mak, K. F. & Law, K. T. Possible topological superconducting phases of MoS_2. *Phys. Rev. Lett.* **113**, 097001 (2014).
15. He, W.-Y. et al. Magnetic field driven nodal topological superconductivity in monolayer transition metal dichalcogenides. Preprint at https://arxiv.org/abs/1604.02867 (2016).
16. Hsu, Y.-T., Vaezi, A., Fischer, M. H. & Kim, E.-A. Topological superconductivity in monolayer transition metal dichalcogenides. *Nat. Commun.* **8**, 14985 (2017).
17. Tinkham, M. *Introduction to Superconductivity* (McGraw-Hill, New York, NY, 2004).
18. Liu, C. X. Unconventional superconductivity in bilayer transition metal dichalcogenides. *Phys. Rev. Lett.* **118**, 087001 (2017).
19. Frigeri, P. A., Agterberg, D. F. & Sigrist, M. Spin susceptibility in superconductors without inversion symmetry. *New J. Phys.* **6**, 115 (2004).
20. Gor'kov, L. P. & Rashba, E. I. Superconducting 2D system with lifted spin degeneracy: mixed singlet–triplet state. *Phys. Rev. Lett.* **87**, 037004 (2001).
21. Yip, S. K. Two-dimensional superconductivity with strong spin–orbit interaction. *Phys. Rev. B* **65**, 144508 (2002).
22. Wakatsuki, R. & Law, K.T. Proximity effect and Ising superconductivity in superconductor/transition metal dichalcogenide heterostructures. Preprint at https://arxiv.org/abs/1604.04898 (2016).
23. Lu, J. M. et al. Evidence for two-dimensional Ising superconductivity in gated MoS_2. *Science* **350**, 1353 (2015).
24. Saito, Y. et al. Superconductivity protected by spin–valley locking in ion-gated MoS_2. *Nat. Phys.* **12**, 144–149 (2015).
25. Nam, H. et al. Ultrathin two-dimensional superconductivity with strong spin–orbit coupling. *Proc. Natl Acad. Sci. USA* **113**, 10513–10517 (2016).
26. Xi, X. et al. Strongly enhanced charge–density–wave order in monolayer NbSe2. *Nat. Nanotec.* **10**, 765–769 (2015).
27. Daghero, D. & Gonnelli, R. S. Probing multiband superconductivity by point-contact spectroscopy. *Supercond. Sci. Technol.* **23**, 043001 (2010).
28. Webb, G. W., Marsiglio, F. & Hirsch, J. E. Superconductivity in the elements, alloys and simple compounds. *Phys. C* **514**, 17–27 (2015).
29. Bianchi, A. et al. First-order superconducting phase transition in $CeCoIn_5$. *Phys. Rev. Lett.* **89**, 137002 (2002).
30. Radovan, H. A. et al. Magnetic enhancement of superconductivity from electron spin domains. *Nature* **425**, 51–55 (2003).
31. Lortz, R. et al. Calorimetric evidence for a Fulde–Ferrell–Larkin–Ovchinnikov superconducting state in the layered organic superconductor κ-$(BEDT\text{-}TTF)_2Cu(NCS)_2$. *Phys. Rev. Lett.* **99**, 187002 (2007).
32. Zocco, D. A., Grube, K., Eilers, F., Wolf, T. & von Löhneysen, H. Pauli-limited multiband superconductivity in KFe_2As_2. *Phys. Rev. Lett.* **111**, 057007 (2013).
33. Kiss, T. et al. Charge-order-maximized momentum-dependent superconductivity. *Nat. Phys.* **3**, 720–725 (2007).

Acknowledgements

This research was supported by the ARO Award W911NF-17-1-0605 for the sample and device fabrication and the US Department of Energy, Office of Basic Energy Sciences contract no. DESC0013883 for the tunelling spectroscopy measurements. A portion of this work was performed at the NHMFL, which is supported by National Science Foundation (NSF) Cooperative Agreement no. DMR-1644779 and the State of Florida. The work in Hong Kong was supported by the Croucher Foundation, the Dr. Tai-chin Lo Foundation and the Hong Kong Research Grants Council through HKUST3/CRF/13G, C6026-16W and 16324216. The work in Lausanne was supported by the Swiss National Science Foundation. We also acknowledge support from the NSF under Award nos DMR-1645901 (E.S.), DMR-1420451 (K.K.) and DMR-1410407 (Z.W.) and a David and Lucille Packard Fellowship and a Sloan Fellowship (K.F.M.).

Author contributions

E.S., J.S. and K.F.M. designed the experiments. E.S. fabricated the devices and performed the measurements with the assistance of S.J., Z.W. and K.K., and of J.-H.P. at the NHMFL. X.X. contributed to all aspects of the experiment in its early phase. W.-Y.H. and K.T.L. performed the theoretical work. H.B. and L.F. synthesized the bulk $NbSe_2$ crystals and screened the sample quality. E.S., W.H., K.T.L., J.S. and K.F.M. analysed the data and co-wrote the paper. All the authors discussed the results and commented on the manuscript.

Competing interests

The authors declare no competing interests.

Additional information

Supplementary information is available for this paper at https://doi.org/10.1038/s41563-018-0061-1.

Reprints and permissions information is available at www.nature.com/reprints.

Correspondence and requests for materials should be addressed to J.S. or K.F.M.

Publisher's note: Springer Nature remains neutral with regard to jurisdictional claims in published maps and institutional affiliations.

Methods

Device fabrication. The NIS junctions employed in this experiment were fabricated using the dry-transfer method[9]. Atomically thin flakes of $NbSe_2$ were mechanically exfoliated onto flexible polydimethylsiloxane (PDMS) substrates from bulk $NbSe_2$ single crystals, which were grown by the vapour-transport method. The thickness of the $NbSe_2$ flakes was first estimated by their optical contrast on PDMS and then verified by their characteristic thickness-dependent superconducting transition temperatures and/or Raman shear-mode frequencies[26]. The identified flakes of appropriate thickness, size and shape were then transferred onto the Si substrates with pre-patterned metal electrodes. Two types of tunnel junction devices have been explored in this study. For the first type, split electrodes of Ti/Pt (4 nm/50 nm) were first deposited on Si/SiO_2 (300 nm) substrates by the standard photolithography and electron-beam evaporation method. The substrates were then cleaned under an ozone environment, followed by electron-beam evaporation of a layer of Al of ~ 0.3–1.5 nm thickness (Supplementary Section 3.1 gives an optimization of the tunnel barrier thickness). The Al layer was allowed to oxidize fully to form AlO_x under ambient conditions for a few hours. To minimize contributions from the electrode resistance to the voltage drop across the junctions, the $NbSe_2$ flakes were aligned and transferred such that one of the sample edges was very close to where the electrodes were split (Fig. 1c). Finally, a thin layer of hexagonal boron nitride (hBN) was transferred on top of the devices as a capping layer. A typical residual resistivity ratio (RRR) of our devices is about 10. For the second type of device, the exfoliated $NbSe_2$ flakes were directly transferred onto pre-patterned Ti/Au (5 nm/50 nm) electrodes. A thin layer (3–4 layers) of an MoS_2 tunnel barrier was then transferred onto the $NbSe_2$ sample, followed by patterning a Ti/Au (5 nm/50 nm) tunnel electrode by electron-beam lithography. The typical RRR (~5) is lower. (Supplementary Sections 3.2, 4 and 5.3 give the results from this type of device).

Transport measurement. Both four-point resistance and differential conductance were measured. In the differential conductance measurements, the junction was biased through one of the split electrodes with a small a.c. bias current, superimposed on a .d.c bias current (the amplitude of the a.c. voltage was kept below 50 μV and the d.c. voltage was varied from −5 mV to 5 mV). Both the a.c. and d.c. voltage drops at the junction were measured through the other electrode of the split pair using a lock-in amplifier and a voltage preamplifier, respectively (Supplementary Section 1 gives the measurement schematic). The differential conductance G was obtained as the ratio of the a.c. current to the a.c. voltage. The d.c. voltage dependence of G is the differential tunelling conductance spectrum reported in the main text. The initial screening of the devices up to 9 T was performed using a Physical Property Measurement System. Measurements under high magnetic fields were performed using the 45 T hybrid magnet at the National High Magnetic Field Laboratory (NHMFL) in a ^{3}He refrigerator with a ^{3}He exchange gas. The hybrid magnet only allows the application of a magnetic field between 11 T and 45 T for most of the temperatures in this study. To apply an in-plane magnetic field with a misalignment of <0.1°, we aligned the devices on a rotating probe such that the four-point resistance was minimized when the magnetic field was fixed slightly below the in-plane upper critical field at the base temperature. This procedure utilizes the large anisotropy in the in-plane and out-of-plane upper critical fields. (Details of the alignment procedure are given in Supplementary Section 2).

Estimate of the in-plane orbital-limited upper critical field. The in-plane orbital-limited upper critical field can be estimated following $H_{c2}^{\parallel}(T=0)=\frac{\sqrt{3}}{\pi}\frac{\Phi_0}{\xi_{\parallel}t}$ (refs [17,25]), where Φ_0, $\xi_{\parallel}$ and t are the flux quantum, in-plane coherence length and sample thickness, respectively. We obtained $H_{c2}^{\parallel}\approx$ 85 T and 170 T, respectively, for trilayer and bilayer $NbSe_2$. In this calculation, we used $\xi_{\parallel}\approx 10$ nm[7] and $t\approx 1.3$ nm (refs [9,26]) for trilayer $NbSe_2$, and $t\approx 0.65$ nm for bilayer $NbSe_2$. These fields far exceed the experimentally measured in-plane upper critical fields (~ 37 T) for both bilayer and trilayer samples. The superconductor–normal metal transition considered here is thus safely in the paramagnetic-limited regime. For simplicity, we neglected the orbital effects in our discussions.

Data availability. The data supporting the plots within this paper and other findings of this study are available from the corresponding authors upon request.